Available online at www.sciencedirect.com
ScienceDirect
Geochimica et Cosmochimica Acta 70 (2006) 6068–6078
Geochimica
www.elsevier.com/locate/gca

Cooling history of lunar Mg-suite gabbronorite 76255, troctolite 76535 and Stillwater pyroxenite SC-936: The record in exsolution and ordering in pyroxenes

I. Stewart McCallum [a,*], M. Chiara Domeneghetti [b], Jeffrey M. Schwartz [a], Emily K. Mullen [a], Michele Zema [b], Fernando Cámara [c], Catherine McCammon [d], Jibamitra Ganguly [e]

[a] *Department of Earth and Space Sciences, University of Washington, Seattle, WA 98195, USA*
[b] *Dipartimento di Scienze della Terra, Università di Pavia, I-27100 Pavia, Italy*
[c] *CNR–Istituto di Geoscienze e Georisorse, Unità di Pavia, I-27100 Pavia, Italy*
[d] *Bayerisches Geoinstitut, Universität Bayreuth, D-95440 Bayreuth, Germany*
[e] *Department of Geosciences, University of Arizona, Tucson, AZ 85721, USA*

Received 9 February 2006; accepted in revised form 9 August 2006

Abstract

We have determined cooling rates of orthopyroxene crystals from two Mg-suite lunar samples (gabbronorite 76255 and troctolite 76535) and one terrestrial sample (orthopyroxenite SC-936 from the Stillwater Complex), on the basis of their Fe–Mg ordering states. In addition, a cooling rate of 76255 was determined by modeling the formation of exsolution lamellae in pyroxenes. The M1–M2 site occupancies of the orthopyroxene crystals were determined by single crystal X-ray diffraction and the rate constant for the ordering reaction was used along with calibrations of the equilibrium intracrystalline fractionation of Fe and Mg as a function of temperature to calculate cooling rates. The closure temperatures (T_C) of cation ordering are ~525 °C for 76255, ~500 °C for 76535 and ~350 °C for SC-936 corresponding to cooling rates of $\sim 4 \times 10^{-2}$ °C/year at the closure temperature for the lunar samples and $\sim 10^{-6}$ °C/year for the Stillwater sample. A cooling rate for 76255, determined by simulating the exsolution process, is 1.7×10^{-2} °C/year at a closure temperature for exsolution of 700 °C. The Fe–Mg ordering cooling rate determined for 76535 reflects a complex thermal history superimposed on the initial plutonic provenance established for this sample [McCallum, I.S., Schwartz, J.M., 2001. Lunar Mg suite: thermobarometry and petrogenesis of parental magmas. *J. Geophys. Res.* **106**, 27969–27983]. The preservation of a crystallization age of 4.51 Ga and a metamorphic age of 4.25 Ga for 76535 is consistent with a model in which excavation of this sample from the lower lunar crust took place while the sample was at a temperature above the closure temperatures for the Sm–Nd, U–Pb and Ar–Ar isotopic systems. Temperatures in excess of the isotopic closure temperatures (i.e., >600 °C) in the lower lunar crust were maintained by heat diffusing from concentrations of U- and Th-rich KREEP material at the base of the crust. On the other hand, 76255 formed at a much shallower depth in the lunar crust (~2 km) and was well below its isotopic closure temperatures at the time of excavation, most likely during the Serenitatis basin-forming impact event. Both lunar samples were reheated during transport to the surface and deposition in hot ejecta blankets. The reheating was short lived but apparently sufficient to redistribute Fe and Mg in M sites in orthopyroxenes. For the lunar samples, the cooling rates based on Fe–Mg ordering represent final stage cooling within an ejecta blanket.

1. Introduction

Rocks of the Mg-suite represent an important component of the pre-4.0 Ga lunar crust and deciphering their petrogenesis is a key to understanding early crustal evolu-

* Corresponding author. Fax: +1 206 543 0489.
E-mail address: mccallum@u.washington.edu (I.S. McCallum).

0016-7037/$ - see front matter © 2006 Elsevier Inc. All rights reserved.
doi:10.1016/j.gca.2006.08.009

tion. The Mg-suite samples form a geochemically coherent group of lunar crustal plutonic rocks and the relationship, if any, of this suite to the other major crustal suite (ferroan anorthosites) has not been firmly established. Most lunar petrologists believe that the Mg-suite rocks crystallized from endogenous magmas produced in the lunar mantle and were emplaced as plutons into the crust shortly after the ferroan anorthosite crust was stabilized. However, the location of these plutons in the early crust is not known and impact-induced mixing during the first 600 million years of lunar history has greatly complicated the task of reconstructing the primary stratigraphy of the lunar crust.

Thermobarometric calculations indicate that Mg-suite troctolite 76535 recrystallized in the lower crust at $T = 800 \pm 50$ °C and a depth of 45 ± 10 km (McCallum and Schwartz, 2001). On the other hand, cooling rates based on modeling the formation of exsolution lamellae in pyroxenes indicate that most samples in the Mg-suite, including gabbronorite sample 76255, formed in relatively shallow level plutons (McCallum and O'Brien, 1996). To extend our knowledge of the cooling history of the Mg-suite samples we have re-determined the cooling rate of 76255 by a refined exsolution modeling method and we have also determined the state of Fe–Mg ordering in orthopyroxenes from lunar samples 76255, 76535 and Stillwater sample SC-936. In the Fe–Mg ordering method, precise knowledge of the intracrystalline distribution of Fe and Mg on the M1 and M2 sites permits the determination of a closure temperature for the ordering process that, in turn, can be used with experimental determination of ordering rates and an asymptotic cooling rate model to constrain the cooling rate at the closure temperature. Typical closure temperatures for the Mg–Fe ordering process are between 300 and 600 °C.

2. Sample description and background

The samples of 76255 provided to us are thin sections of light-colored clasts extracted from a $6\,\text{cm} \times 4\,\text{cm}$ impact melt breccia chipped from the Apollo 17, station 6 boulder (Simonds et al., 1974). The mineral and lithic fragments in the sections have been cataclasized but they form a monomict assemblage derived from a relatively coarse-grained gabbronorite source rock (Warner et al., 1976). In the thin sections examined by us, most clasts are optically clear and unshocked. The most abundant mineral clasts are unshocked plagioclase with oscillatory zoning, clear crystals of augite with lamellae of pigeonite on (001) and (100), and clear crystals of orthopyroxene formed by the inversion of primary pigeonite. The orthopyroxene grains contain relict "001" exsolution lamellae of augite and post inversion lamellae of augite on (100). The textures in pyroxenes from 76255 are reminiscent of textures observed in pyroxenes from the lower part of the Skaergaard Intrusion. Although there appear to be only minor compositional and textural effects on mineral clasts from incorporation in a hot impact melt sheet, it would seem highly probable that there were significant thermal effects. The poikilitic and ophitic texture of the inter-clast matrix of station 6 boulder samples is indicative of the presence of a melt phase at the time of deposition (Warner et al., 1976). The relatively short-lived heating event associated with incorporation of "cold" clasts in an impact melt was followed by a longer cooling event after the melt sheet was deposited. Petrographic evidence suggests that the larger clasts maintained their macroscopic integrity throughout this process while adjusting on the submicroscopic scale.

Sample 76535 is a texturally and compositionally pristine, coarse-grained, plutonic troctolite collected at station 6 as part of a rake sample. Other troctolitic clasts (usually less well preserved) occur at station 6 as clasts in melt breccias and as rake samples indicating that a troctolitic pluton was excavated by the Serenitatis impact. 76535 has been described as an olivine–plagioclase cumulate (Dymek et al., 1975) but metamorphic textures and an equilibration temperature of 800 °C provide clear evidence of extensive recrystallization (McCallum and Schwartz, 2001). The sample contains roughly equal modal amounts of olivine and plagioclase while orthopyroxene makes up ~4% of the rock. A symplectite with two pyroxenes + chrome spinel has formed at olivine–plagioclase contacts, and using an olivine–orthopyroxene–clinopyroxene–plagioclase–spinel thermobarometer, McCallum and Schwartz (2001) determined a burial depth of 45 ± 10 km. Clear crystals of orthopyroxene with no optically visible exsolution features were separated from both 76255 and 76535 for the X-ray study.

To determine if the orthopyroxene cooling rate chronometer is applicable to terrestrial pyroxenes with a reasonably well-known thermal history, Mg and Fe site occupancies were determined on orthopyroxene crystals from a Stillwater orthopyroxenite (SC-936). The Stillwater pyroxenes are homogeneous, approximately the same composition as those in 76535, and they contain optically visible (100) clinopyroxene exsolution lamellae.

3. Experimental and analytical methods and results

3.1. X-ray single-crystal diffraction study

We have determined the Fe–Mg site distribution of two orthopyroxene crystals in sample 76255, two from sample 76535, and one from sample SC-936 by X-ray single crystal diffraction methods as described by Ganguly and Domeneghetti (1996). An important result of this study is that reflections from small amounts of clinopyroxene exsolved on (100), which may not be visible optically, were recognized and corrected for. X-ray intensity data were obtained with a conventional Philips PW 1100 four-circle automated diffractometer (graphite-monochromatized MoKα radiation $\lambda = 0.71073$ Å) by measuring step-scan profiles and analyzing them by the Lehmann and Larsen (1974) σ_I/I method. The presence of (*0kl*) "forbidden reflections" with $k = 2n + 1$ and $l = 4n + 2$, having $I \geqslant 3\sigma_I$ is consistent

with reflections from $C2/c$ clinopyroxene exsolved on (100) and superimposed on the ($0kl$) "forbidden reflections" of the orthopyroxene. All diffraction effects of $C2/c$ augite are superimposed on those of *Pbca* orthopyroxene with $(h + k) = 2n$, and this overlap explains the monoclinic-like equivalence of the collected reflections. Reflections hkl, $\overline{h}kl$, $h\overline{k}l$ and $\overline{hk}l$ were measured up to $\theta \leqslant 35°$ in the $\omega - 2\theta$ scan mode. The intensities were corrected for absorption using the semi-empirical method of North et al. (1968) and the values of the equivalent pairs in $2/m$ Laue symmetry (hkl and $h\overline{k}l$, $\overline{h}kl$ and $\overline{hk}l$) were averaged. The cell parameters were determined by centering 60 reflections, using a locally improved version of the Philips LAT routine and are reported in Table 1.

The structure refinement was carried out following the procedure of Domeneghetti et al. (1996) for a *Pbca* phase coexisting with a $C2/c$ exsolved phase. The calculated fraction of the $C2/c$ phase is about 1% for both 76535 and 76255 samples and 3% for SC-936 sample. In both lunar and terrestrial orthopyroxenes, the violations of *Pbca* extinction conditions are due to (100) exsolved augite and not to a lower symmetry $P2_1ca$ phase as has been suggested for lunar sample 76535 (Smyth, 1974, 1975; Steele, 1975). The observed F_o^2 values, corrected for the contribution from the augite, were then treated with a full-matrix least-squares refinement by SHELX-97 (Sheldrick, 1998), using individual weights and the weighting scheme suggested by the program. The atomic scattering curves were taken from *International Tables for X-ray Crystallography* (Ibers and Hamilton, 1974). The extinction correction was applied with the procedures of program SHELX-97. The program initially provides the average of F_o^2 values of equivalent pairs in *mmm* Laue symmetry (hkl and $\overline{h}kl$) and the relevant discrepancy factor R_{int}, is reported in Table 1 together with the number of total and independent reflections. The number of observed reflections, the index R_{all} based on all the F_o^2, the discrepancy index R_1 based on $F_o^2 > 2\sigma(F_o^2)$, and the goodness of fit (S) are reported in Table 2 along with the mean atomic numbers (m.a.n.) at M1 and M2 sites and the mean bond distances of SiA, SiB, M1 and M2 polyhedra. Atomic positions and anisotropic displacement parameters are reported in electronic annex EA-1.

3.2. Mössbauer analysis

To determine Fe^{3+}/Fe_T, crystals of 76535 and SC-936 orthopyroxenes were mounted between pieces of cellophane tape for easy handling. A 400 μm diameter hole was drilled in a piece of 25 μm thick Ta foil (absorbs 99% of 14.4 keV gamma rays) and placed over the central part of the sample under microscopic observation. Absorber thicknesses were estimated to be approximately 4 mg Fe/cm^2 and 7 mg Fe/cm^2 for the lunar and Stillwater crystals, respectively. Mössbauer spectra were recorded at room temperature (20 °C) in transmission mode on a constant acceleration Mössbauer spectrometer with a nominal 10 mCi ^{57}Co high specific activity source in a 12 μm Rh matrix. The velocity scale was calibrated relative to 25 μm α-Fe foil using the positions certified for (former) National Bureau of Standards standard reference material 1541; line widths of 0.34 mm/s for the outer lines of α-Fe were obtained at room temperature. The spectra were fitted using the commercially available fitting program NORMOS written by R.A. Brand (distributed by Wissenschaftliche Elektronik GmbH, Germany). Spectra took approximately one week each to collect. The Fe^{3+}/Fe_T ratios for samples 76535 and SC-936 were $0.0 \pm 1\%$ and $4.5 \pm 1.5\%$, respectively, i.e., there was no evidence for Fe^{3+} in the spectrum of the lunar sample within the detection limit (1%). The Mössbauer spectra for samples 76535 and SC-936 are shown in Fig. 1.

3.3. Electron microprobe analysis

To ensure high accuracy of the site occupancy determinations, the compositions of all X-rayed crystals, except sample 76535 N.2, which was lost during polishing, were determined by averaging the results of a large number of electron microprobe spot analyses carried out on a JEOL 733 at the University of Washington (samples 76535 and SC-936) and a Cameca SX50 at the University of Arizona (sample 76255). Synthetic and natural pyroxenes were used as standards. Orthopyroxenes in lunar samples 76535 and 76255 are homogeneous. However, initial analyses of Stillwater sample SC-936 showed a range of Ca contents from 0.047 to 0.132 atoms per 6 oxygens due to the presence of

Table 1
Unit cell parameters, details on data collection and structure refinements of crystals from samples SC-936, 76535 and 76255

	a (Å)	b (Å)	c (Å)	V (Å^3)	θ range (°)	I_{tot}	I_{ind}	R_{int} (%)	Dimension (mm)
SC-936 N1	18.258(4)	8.836(3)	5.198(2)	838.6	3–35	3657	1854	1.60	$0.13 \times 0.26 \times 0.33$
76535 N1	18.265(12)	8.838(5)	5.198(7)	839.0	3–35	3646	1848	1.63	$0.33 \times 0.43 \times 0.51$
76535 N2	18.273(10)	8.841(5)	5.199(4)	839.8	3–35	3654	1854	1.86	$0.21 \times 0.41 \times 0.43$
76255 N1	18.308(5)	8.890(3)	5.219(2)	849.5	2–35	3704	1879	2.24	$0.41 \times 0.41 \times 0.64$
76255 N2	18.311(7)	8.889(4)	5.219(2)	849.5	2–35	3716	1887	1.43	$0.36 \times 0.40 \times 0.73$

Notes: standard deviations are given in parentheses.
I_{tot} is the total number of reflections after merging for 2/m symmetry.
I_{ind} is the number of independent reflections used for the structure refinement.
$R_{int} = \sum |F_o^2 - F_o^2(\text{mean})| / \sum [F_o^2]$.

Table 2
Structural parameters of crystals from samples SC-936, 76535 and 76255

	R_{all} (%)	R_1 (%)	I_{obs}	S	% $C2/c$	m.a.n. M1	m.a.n. M2	m.a.n. M1 + M2	<SiA–O>	<SiB–O>	<M1–O>	<M2–O>
SC-936 N1	4.14	3.20	1552	1.156	3.11	12.49(4)	16.24(4)	28.73	1.627	1.644	2.077	2.169
SC-936 N1 Ca-reduct.	4.14	3.20	1552	1.157	3.11	12.49(4)	16.22(4)	28.71	1.627	1.644	2.077	2.169
76535 N1	3.57	2.78	1620	1.182	1.12	12.57(3)	15.31(4)	27.88	1.629	1.645	2.077	2.167
76535 N1 Ca-reduct.	3.58	2.78	1620	1.178	1.12	12.54(3)	15.23(4)	27.77	1.629	1.645	2.077	2.167
76535 N2	3.69	2.90	1620	1.229	0.94	12.59(3)	15.33(4)	27.92	1.629	1.645	2.078	2.168
76535 N2 Ca-reduct.	3.70	2.91	1620	1.226	0.94	12.55(3)	15.25(4)	27.80	1.629	1.645	2.078	2.168
76255 N1	3.41	2.68	1654	1.162	1.40	13.46(3)	20.14(4)	33.60	1.627	1.641	2.086	2.198
76255 N2	3.78	2.81	1622	1.232	1.90	13.46(3)	20.20(5)	33.66	1.627	1.641	2.086	2.197

Notes: Standard deviations in the mean atomic number (m.a.n.) columns are given in parentheses.
$R_{all} = \sum ||F_o| - |F_c|| / \sum |F_o|$.
$R_1 = \sum ||F_o| - |F_c|| / \sum |F_o|$ for $F_o^2 > 2\sigma(F_o^2)$.
$S = [\sum [w(F_o^2 - F_c^2)^2] / (n-p)]^{0.5}$, where n is the number of reflections and p is the total number of parameters refined.
I_{obs} is the number of independent reflections with $F_o^2 > 2\sigma(F_o^2)$.

Fig. 1. Room temperature Mössbauer spectra of orthopyroxene single crystals from (a) lunar troctolite 76535; and (b) Stillwater SC-936. Absorption corresponding to Fe^{3+} is shaded grey. The residual and subspectral components are shown above each spectrum, and are shifted vertically for clarity. Note the absence of Fe^{3+} in the lunar sample.

augite lamellae up to 1 μm wide. To avoid the lamellae effect, the analyses reported were obtained on a lamellae-free zone at the rim of the crystal. Analyses are listed in Table 3 (averaged column). The average compositions were mathematically projected on to a surface that satisfies the crystal chemical constraints of orthopyroxene (Dollase and Newman, 1984; Stimpfl et al., 1999). These optimized compositions (Table 3, optimized column) were used in the site occupancy refinements in which the dilute non-binary components (Ca, Mn, Cr, Ti and Al) were treated according to the method of Ganguly and Domeneghetti (1996). For crystals SC936-N1 and 76535-N1, the Ca content was adjusted to correct for the effects of the Guinier-Preston Zones (GPZ) (Table 3, Ca reduction column).

The compositions of bulk pyroxenes in 76255 were determined by recombining host and lamellae in proportions determined from back scattered electron (BSE) images such as that shown in Fig. 2a. Coexisting pyroxenes indicate an initial temperature of formation for 76255 of ~1100 °C, while the compositions of adjacent host–lamellae pairs indicate a closure temperature of ~700 °C for sub-

Table 3
Initial and optimized compositions of orthopyroxene samples SC-936, 76535 and 76255

	SC-936 N1			76535 N1			76255 N1		76255 N2	
	Averaged	Optimized	Ca reduction	Averaged	Optimized	Ca reduction	Averaged	Optimized	Averaged	Optimized
SiO_2 (wt %)	55.12	55.48	55.49	55.64	55.91	55.96	52.90	52.86	52.88	52.85
TiO_2	0.22	0.23	0.23	0.46	0.47	0.47	0.75	0.71	0.76	0.70
Al_2O_3	1.49	1.50	1.52	1.43	1.46	1.56	0.68	1.03	0.69	1.02
Cr_2O_3	0.37	0.37	0.37	0.73	0.73	0.73	0.29	0.26	0.29	0.27
MgO	31.04	31.12	31.30	32.28	32.33	32.70	23.01	23.04	23.03	23.00
FeO	9.74	9.74	9.84	7.38	7.41	7.43	19.76	19.74	19.97	19.91
Fe_2O_3	0.51	0.52	0.53	0.00	0.00	0.00	0.00	0.00	0.00	0.00
MnO	0.20	0.20	0.20	0.14	0.14	0.14	0.29	0.29	0.30	0.30
CaO	0.83	0.82	0.50	1.54	1.54	0.96	2.13	2.04	1.99	1.91
Na_2O	0.02	0.02	0.02	0.03	0.03	0.05	0.02	0.03	0.02	0.04
Total	99.54	100.00	100.00	99.65	100.00	100.00	99.83	100.00	99.93	100.00
Cations/6 O										
Si	1.9487(48)	1.9513	1.9509	1.9470(60)	1.9488	1.9476	1.9611(23)	1.9553	1.9597(22)	1.9555
Al^{IV}	0.0484(48)	0.0487	0.0491	0.0505(60)	0.0512	0.0524	0.0297(22)	0.0447	0.0302(22)	0.0445
Al^{VI}	0.0138(59)	0.0135	0.0140	0.0087(63)	0.0085	0.0115	0.0000	0.0000	0.0000(25)	0.0000
Ti	0.0060(11)	0.0061	0.0060	0.0121(10)	0.0122	0.0122	0.0209(4)	0.0197	0.0212(5)	0.0196
Cr	0.0103(15)	0.0104	0.0104	0.0201(10)	0.0201	0.0201	0.0085(4)	0.0077	0.0085(4)	0.0080
Mg	1.6359(127)	1.6318	1.6404	1.6838(110)	1.6798	1.6963	1.2715(47)	1.2703	1.2722(53)	1.2687
Fe^{2+}	0.2880(72)	0.2864	0.2892	0.2160(20)	0.2159	0.2164	0.6126(48)	0.6105	0.6189(56)	0.6160
Fe^{3+}	0.0135(45)	0.0138	0.0140	0.0000	0.0000	0.0000	0.0000	0.0000	0.0000	0.0000
Mn	0.0060(4)	0.0059	0.0059	0.0041(2)	0.0040	0.0040	0.0091(6)	0.0092	0.0094(6)	0.0095
Ca	0.0313(30)	0.0309	0.0189	0.0579(30)	0.0577	0.0359	0.0846(63)	0.0809	0.0791(74)	0.0756
Na	0.0012(4)	0.0012	0.0012	0.0024(30)	0.0018	0.0036	0.0014(5)	0.0019	0.0014(6)	0.0026
Total	4.0029	4.0000	4.0000	4.0026	4.0000	4.0000	3.9996	4.0000	4.0005	4.0000
Charge	12.0000	12.0000	12.0000	12.0000	12.0000	12.0000	12.0000	12.0000	12.0000	12.0000
d(M − T)	0.0000	0.0000	0.0000	0.0000	0.0000	0.0000	0.0000	0.0000	0.0000	0.0000
M-cations	2.0058	2.0000	2.0000	2.0051	2.0000	2.0000	2.0086	2.0000	2.0107	2.0000
T-cations	1.9971	2.0000	2.0000	1.9975	2.0000	2.0000	1.9908	2.0000	1.9899	2.0000

Notes: Standard deviations are given in parentheses.
d(M − T) = difference between the charge excess in M site and the charge deficiency in T site.

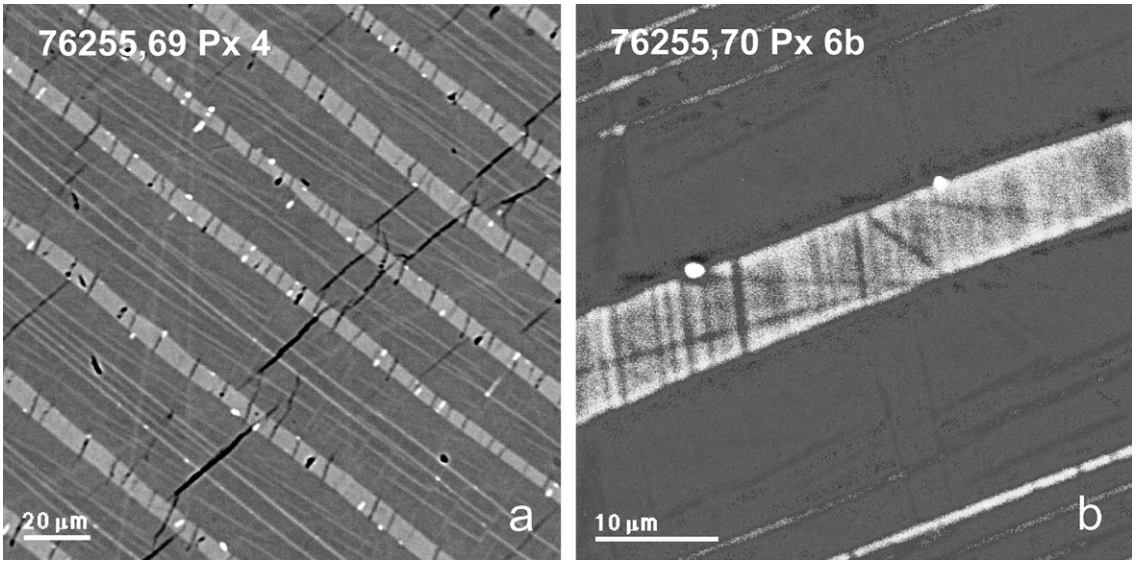

Fig. 2. Backscattered electron images of 76255. (a) BSE image of augite grain showing exsolution of pigeonite lamellae on (001) of the host augite. Small bright spots are oxide grains. (b) BSE image of a single (001) pigeonite lamella in an augite host. The entire area scanned in wavelength disperse mode and the measured profile (shown in Fig. 3) is selected from the data set.

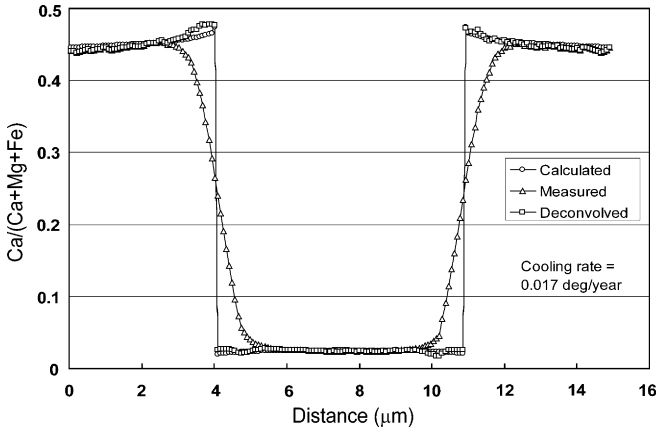

Fig. 3. Measured, deconvolved, and calculated profiles in clinopyroxene crystal with pigeonite lamella on (001). Calculated profile based on *average* cooling rate of 0.022 °C/year.

micron-scale Ca–FeMg diffusion (see McCallum and O'Brien, 1996; for plots of the data).

To compute compositional profiles across host–lamellae pyroxene pairs, Fe, Mg, Ca and Al wavelength dispersive (WDS) X-ray maps were obtained on augite grains with (001) pigeonite lamellae oriented perpendicular to the plane of the section. A small area is scanned for several hours and compositional profiles are determined by selecting areas on the X-ray maps as shown in Fig. 2b. Counts in each pixel were converted to wt% oxide using correction factors obtained from conventional probe analyses of individual host and lamellae pairs. This method provides a much larger set of compositional data that greatly improves corrections for beam overlap effects. This correction is required because in the vicinity of a lamellae–host interface the measured composition represents a weighted average of the volume of sample excited by the electron beam (Ganguly et al., 1988). The magnitude of the overlap effect is different for different elements and is primarily a function of the excitation voltage. The volume of excitation around the incident beam is assumed to have a radially symmetric Gaussian intensity distribution with a standard deviation (ε) which can be calculated from the slope of the measured profile at the interface. We follow the method of Ganguly et al. (1988) in which a hypothetical concentration profile is convolved and the correction factors obtained from this convolution are applied to the measured profile. In practice, it is usually only necessary to correct the raw data for a distance of a few micrometers on either side of the interface. Fig. 3 shows a measured and deconvolved profile for an exsolved augite from 76255. The effect of spatial averaging by the electron beam is significant and attempts to model profiles without first deconvolving them are subject to large errors.

3.4. TEM studies

TEM observations were made on orthopyroxene crystals from 76535 and SC-936 using a JEOL 200 kV electron microscope with a LaB_6 electron source at the Dipartimento di Scienze della Terra at the Siena University, Italy. The microscope is equipped with an Oxford ISIS system for EDS microanalysis incorporating a Li-doped silicon detector with an ultra-thin window. The crystals were oriented with the b^*-axis perpendicular to the sample surface, ground on both sides with SiC, finished with diamond paste, glued to copper rings and thinned to electron transparency by ion milling with an argon beam. The electron beam size was ~5 nm, and the live time is 50 s. Analyses were obtained by the Cliff-Lorimer method using Si as a standard element and determining oxygen by stoichiometry.

Conventional contrast imaging in bright field (BF) and dark field (DF) of orthopyroxene crystals show augite exsolution lamellae parallel to $(100)_{Opx}$ in all samples and the ubiquitous presence of Guinier-Preston zones (GPZ) (Champness and Lorimer, 1973; Nord, 1980). In sample SC-936 [GPZ-free composition = $Wo_1En_{83}Fs_{16}$] augite lamellae (~5 modal % $Wo_{50}En_{44}Fs_6$) are 50–70 nm thick

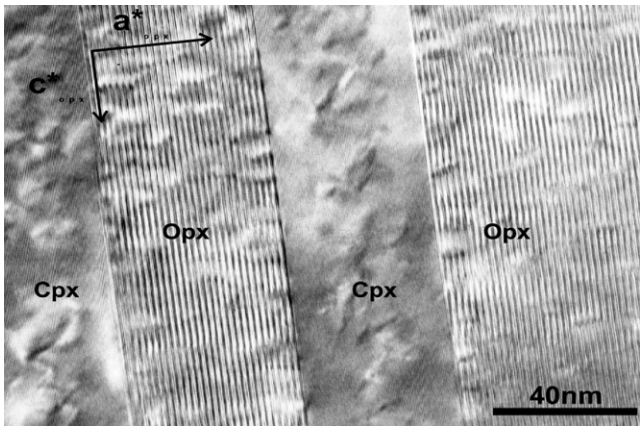

Fig. 4. TEM image of Stillwater orthopyroxene SC-936 with (100) clinopyroxene exsolution lamellae ~50 nm in width. Zone axis is [010]. Lamellae make up ~5% of the orthopyroxene.

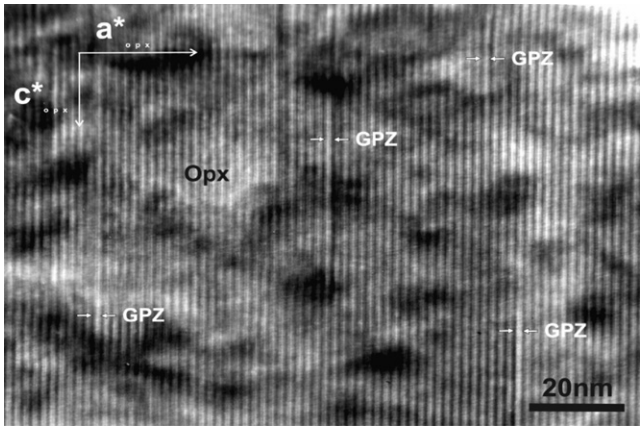

Fig. 5. High-resolution image of Stillwater pyroxene SC-936 showing the development of pervasive Guinier-Preston Zones (GPZ) indicated by arrows. Zone axis is [010]. The GPZ are one a^* (orthopyroxene) wide and ~100 nm in length.

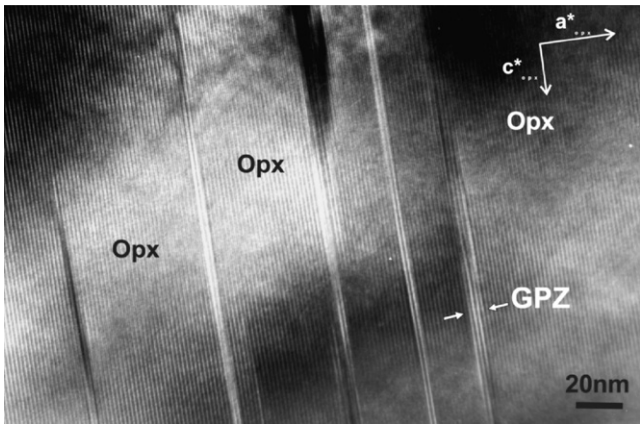

Fig. 6. High-resolution image of lunar troctolite 76535 showing the development of Guinier-Preston Zones (GPZ). Zone axis [010]. The GPZ show a different contrast but the same periodicity along a^* and they are several a^* (orthopyroxene) wide.

with a few narrow (~5 nm) sets (Fig. 4). In 76535, augite lamellae are less abundant, <10 nm thick, and have a limited *c*-axis development. Orthopyroxene in 76535 also contains oriented chromite inclusions in which $(100)_{Opx}$ // $\{111\}_{Chr}$, $(010)_{Opx}$ // $\{101\}_{Chr}$ and $(001)_{Opx}$ // $\{121\}_{Chr}$ as reported by Cámara et al. (2000) in Johnstown orthopyroxene.

In crystals from sample SC-936, GPZ are one orthopyroxene *a*-lattice wide with variable *c*-lattice length (~100 nm) (Fig. 5) whereas in crystals from sample 76535, GPZ are several orthopyroxene *a*-lattice thick (Nord, 1980) and shorter along the *c*-lattice with a characteristic oblique termination and stronger strain contrast (Fig. 6). High-resolution imaging of GPZ with the electron beam parallel to [010] shows phase contrast change and a slight *a*-lattice variation. Analysis of GPZ in crystals from sample 76535 with a small probe (nominally ~3 nm) yielded a composition of $Wo_5En_{79}Fs_{16}$ [cf. GPZ-free orthopyroxene composition = $Wo_1En_{84}Fs_{15}$]. The error in this analysis for Ca is large (~30% 1σ) but the difference with GPZ-free orthopyroxene is larger than the analytical uncertainty. If this analysis is representative, the GPZ may represent a Ca-rich orthopyroxene structure as previously proposed by Nord (1980). Cámara et al. (2000) performed line profile analyses in Johnstown orthopyroxene and reported a relative minimum enrichment of 40% of Ca in GPZ.

Selected area electron diffraction (SAED) shows streaking along a^* and spot splitting on (*h*00) at high resolution [first visible on $(800)_{opx}$] due to a larger *a*-lattice of augite as described by Cámara et al. (2000) from the Johnstown diogenite. The streaking is due to the presence of GPZ (with variable {100} spacing), while splitting is due to augite exsolution. After annealing for 234 h at 1100 °C, crystals from sample SC-936 are essentially devoid of GPZ. However, the exsolution lamellae are still present and essentially the same composition. Due to the effect of GPZ, we have made a correction to the Ca content of the orthopyroxenes in all samples. The corrections reduce

Table 4
Cation distribution, k_D and T_c values of crystals SC-936, 76535 and 76255

	SC-936 N1 Optimized	SC-936 N1 Ca reduction	76535 N1 Optimized	76535 N1 Ca reduction	76535 N2 Optimized	76535 N2 Ca reduction	76255 N1 Optimized	76255 N2 Optimized
TB site								
Si	1.9513	1.9509	1.9488	1.9476	1.9488	1.9476	1.9553	1.9555
Al	0.0487	0.0491	0.0512	0.0524	0.0512	0.0524	0.0447	0.0445
M1 site								
Mg	0.9492(28)	0.9494(28)	0.9446(25)	0.9450(25)	0.9441(25)	0.9449(25)	0.8888(18)	0.8888(21)
Fe	0.0070(31)	0.0062(31)	0.0146(17)	0.0114(17)	0.0158(18)	0.0122(18)	0.0840(18)	0.0837(21)
Fe^{3+}	0.0138	0.0140	—	—	—	—	—	—
Al	0.0135	0.0140	0.0085	0.0115	0.0075	0.0098	—	—
Cr	0.0104	0.0104	0.0201	0.0201	0.0203	0.0206	0.0077	0.0080
Ti	0.0061	0.0060	0.0122	0.0122	0.0123	0.0125	0.0197	0.0196
M2 site								
Mg	0.6821(26)	0.6891(26)	0.7370(26)	0.7493(26)	0.7345(26)	0.7472(26)	0.3811(24)	0.3782(27)
Fe	0.2801(30)	0.2849(30)	0.2004(19)	0.2062(19)	0.2012(19)	0.2070(19)	0.5272(29)	0.5338(35)
Ca	0.0309	0.0189	0.0577	0.0359	0.0585	0.0385	0.0809	0.0756
Mn	0.0059	0.0059	0.0040	0.0040	0.0040	0.0040	0.0092	0.0095
Na	0.0012	0.0012	0.0018	0.0036	0.0018	0.0033	0.0019	0.0026
X_{Fe}^{M1}	0.0073	0.0065	0.0152	0.0119	0.0165	0.0127	0.0863	0.0861
X_{Fe}^{M2}	0.2911	0.2925	0.2138	0.2158	0.2150	0.2169	0.5804	0.5853
k_D	0.0179	0.0158	0.0568	0.0438	0.0611	0.0466	0.0683	0.0667
T_c (K)	626	610	825	770	842	782	801	796
T_c (°C)	353	337	552	497	569	509	528	523

Notes: Standard deviations are given in parentheses.
$X_{Fe}^{M1} = Fe_{M1}/(Fe + Mg)_{M1}$; $X_{Fe}^{M2} = Fe_{M2}/(Fe + Mg)_{M2}$.
$k_D = X_{Fe}^{M1}[1 - X_{Fe}^{M2}]/X_{Fe}^{M2}[1 - X_{Fe}^{M1}]$.

the closure temperatures by ~60 °C for the lunar samples and ~20 °C for the Stillwater sample (Table 4).

3.5. Ordering states and closure temperatures

For sample SC-936, the average composition of the lamella-free zone at the grain edge was used and the effect of the Fe^{3+}, determined by Mössbauer analysis, was included in the site occupancy determination. For the lunar crystal 76535 N2 that was lost, the compositional data obtained on crystal N1 were used. For both crystals we also calculated an optimized composition in which the Ca content was reduced by 40% because of the presence of GPZ (Cámara et al., 2000). The resulting bulk compositions were used as linear constraints, together with their standard deviations, in the final least-squares cycles of the structure refinement by SHELX-97. As the Mn content of the three samples is very low (<0.010 atoms/6 oxygens), the site distribution was obtained by considering Mn to be totally ordered in M2 according to Stimpfl (2005). The M1 site population was then checked by comparing the value of the observed M1–O mean bond distance obtained by the structure refinement with that calculated by using equation (21) from Domeneghetti et al. (1995). For the three crystals of samples SC-935 and 76535 the agreement was within the estimated standard deviations (0.001 Å) while a calculated value of 2.083 Å instead of 2.086 Å was obtained for both crystals of sample 76255. This difference can be ascribed to an insufficient correction for the influence of the M2 site population, provided by equation (21), in the presence of a high Ca content.

The site populations and Fe–Mg exchange distribution (k_D) values for crystals SC-936 N1 and for crystals N1 and N2 of lunar samples 76535 and 76255 are reported in Table 4 together with data obtained after Ca reduction by 40%. Closure temperatures (T_C) (Table 4) based on the cation ordering were calculated according to calibrations of Stimpfl et al. (2005). For SC-936 and 76535 orthopyroxenes, the equation for the low-iron sample ST5 (Fs_{16}) was used while for 76255 orthopyroxene that for the intermediate-iron sample HO (Fs_{50}) was used. It is worth noting that the k_D values obtained using the "Ca-reduced" data are consistent for all samples with more ordered Mg/Fe distributions, thus providing lower T_C values.

4. Cooling rates

The cooling rates were determined from (a) orthopyroxene ordering data and (b) host–lamellae composition profiles in clinopyroxene. These chronometers record diffusion on different length scales and consequently have different closure temperatures. For the orthopyroxene chronometer, we used the numerical method and code (CRATE) of Ganguly (1982) that uses Mueller's theory (Mueller, 1967) of order–disorder kinetics. The cooling was assumed to follow an asymptotic law, namely

$$1/T = 1/T_o + \eta t$$

where η is a cooling time constant ($K^{-1}t^{-1}$), and T_o is the initial temperature. In this model the cooling rate depends on T according to $dT/dt = -\eta T^2$. The numerical code was updated using the thermodynamic and kinetic data for the intracrystalline exchange of Fe and Mg in orthopyroxene from Stimpfl et al. (2005). Both lunar samples show a cooling rate of ~0.04 °C/year near the closure temperature of 500–530 °C (Table 4). The composition of the orthopyroxene in 76535 is slightly outside the range over which the geochronometer has been experimentally calibrated and therefore this cooling rate is subject to a larger uncertainty. On the other hand, the Stillwater orthopyroxene datum gives a cooling rate of ~1 °C/My near the closure temperature of 340 °C, for fO_2 between the WI and QFM buffers, assuming an $(fO_2)^{1/6}$ dependence of the rate constant (Stimpfl et al., 2005).

A cooling rate for gabbronorite sample 76255 was independently determined by modeling the formation of pigeonite exsolution lamellae in augite using the method described in McCallum and O'Brien (1996) and Jolliff et al. (1999). The closure temperature of lamellae formation is estimated to be ~700 °C based on the pyroxene interface compositions and the Sack and Ghiorso (1994) solvus. Since the (001) lamellae in augite and pigeonite grow along a planar front by interdiffusion of Ca and MgFe parallel to the c axis, a one dimensional solution to the diffusion equation is sufficient. To simulate lamellae growth, we use a numerical solution to the diffusion equation which allows for compositional and temperature-dependent diffusion coefficients. The Ca–Mg interdiffusion coefficients were calculated from the Ca and Mg tracer diffusion results of Stimpfl et al. (2003) measured at 900 °C and 1000 °C. These results were extrapolated to lower temperatures on a $\log D$ versus $1/T$ plot. The interdiffusion of Ca and FeMg in pyroxene should also depend on the Mg/(Mg + Fe) ratio since the tracer diffusivities of Fe and Mg are likely to be different, as suggested by the analysis of Ganguly and Tazzoli (1994) for Fe–Mg diffusion in orthopyroxene, but there are insufficient data to assess this effect. An exponential cooling model was used to calculate the cooling rate. In the simulation of compositional profiles, it is necessary to specify the locus of the solvus in temperature-composition space, an appropriate field length for diffusion (i.e., half width of a lamella plus the half width of an adjacent host measured on the crystal), bulk Ca/(Ca + Mg + Fe) and Fe/(Mg + Fe) of the pyroxene, and the closure temperature for diffusion. An analysis of errors involved in the exsolution simulations indicates an uncertainty of about a factor of ~100% in the retrieved cooling rate values (Jolliff et al., 1999). The best-fit calculated exsolution profile gives an average cooling rate of 0.017 °C/year at the closure temperature of 700 °C (Fig. 3). The same cooling path continued to the closure temperature for ordering would result in a cooling rate of 0.002 °C/year at 525 °C, i.e., a rate significantly lower than that measured

by the orthopyroxene chronometer. Because lunar troctolite 76535 was not saturated with two pyroxenes at the solidus, it is not possible to apply the exsolution-diffusion chronometer to this sample.

5. Discussion

The Stillwater cooling rate of ~1 °C/Ma has a large uncertainty but it is much lower than computed cooling rates for a mid-crustal terrestrial intrusion (Irvine, 1970). However, the Stillwater complex was subjected to a low-grade (greenschist facies) metamorphic event at 1.7 Ga, the effects of which can be observed in the development of secondary minerals along fractures and in disturbances of the U–Pb (McCallum et al., 1999) and Rb–Sr (DePaolo and Wasserburg, 1979) isotopic systems. Heating associated with the metamorphic event would induce intracrystalline redistribution of Fe and Mg, and it is likely that the low closure temperature of SC-936 is reflecting this later low-temperature heating event.

The cooling history of a sample from an igneous intrusion is dependent on several factors, specifically; the temperature of the magma at intrusion; the temperature of the country rock; the dimensions and shape of the intrusion; the thermal conductivity of the magma, its crystalline equivalent, and the country rock; the latent heat of crystallization; the location of the sample in the intrusive body; and the extent to which convection is operative. Determination of the depth at which a particular sample cooled is dependent on the boundary conditions chosen and there is no unique solution based on cooling rate alone. The cooling rate of the gabbronorite sample 76255 determined from modeling the exsolution process is 0.017 °C per year at a closure temperature of ~700 °C and we interpret this rate as the initial cooling event in a plutonic magmatic environment. This rate could correspond to cooling in the center of a sill one kilometer thick intruded at 1200 °C at a depth ~1.8 km within the Moon with country rock temperature of 300 °C, assuming a thermal diffusivity of 31.5 m^2/year, a typical value for solid rock or magma. At depths in excess of a few kilometers, the size of the intrusion and the temperature of the country rock are the main determinants of the cooling rate but all reasonable models give emplacement depths of ~1–2 km for 76255. The extent to which the primitive lunar crust is brecciated also plays a role since the thermal conductivity of brecciated and porous material is significant lower than that of solid rock. Given these considerations, a single cooling rate can provide non-unique results and a better approach is to use cooling rate indicators with different closure temperatures, or independent indicators of emplacement depths. However, in the case of gabbronorite 76255, the period of initial cooling in an intrusion emplaced in the upper lunar crust was followed by a reheating event and more rapid cooling. Given the occurrence of 76255 as a clast in the station 6 impact melt breccia, we conclude that the reheating and subsequent cooling that is recorded in the Fe–Mg ordering rate is associated with the incorporation of the clast in the impact melt followed by emplacement and cooling of the breccia on the lunar surface. A single Ar–Ar age determination on clast 76255,46 by Cadogan and Turner (1976) gave an age of 4.02 ± 0.04 Ga that is indistinguishable from the age of the Serenitatis basin-forming event, suggesting that the Ar–Ar clock in 76255 was reset by this event. This same event would certainly produce Mg–Fe disorder in the orthopyroxenes in 76255 while leaving the exsolution textures intact (Ganguly and Tazzoli, 1994). Impact melt breccias are relatively coherent rocks with variable porosity and it is likely they would have a thermal diffusivity less than that of solid rock but greater than porous regolith. Using a thermal diffusivity of 2.32 m^2/year as suggested by Warren et al. (1991) for the lunar megaregolith, cooling at the rate of 0.04 °C/year at the closure temperature of 525 °C as indicated by the Fe–Mg ordering chronometer requires burial to a depth of ~200 m. This depth is within the thickness range calculated for the proximal facies of the ejecta blanket associated with the Serenitatis basin-forming event.

Interpretation of the Fe–Mg ordering cooling rate result for troctolite 76535 presents a different problem. Thermobarometric calculations give a T of 800 °C and P of 2.2–2.5 kb for 76535, confirming this sample as one of the few pristine deep-seated lunar crustal rocks (McCallum and Schwartz, 2001). However, all realistic models of cooling of intrusions emplaced at a depth of ~40 km in the Moon give cooling rates that are at least an order of magnitude lower than that indicated by the orthopyroxene chronometer for 76535. The latest stage cooling of this sample apparently took place fairly rapidly in a near-surface environment. Rapid cooling through the closure temperature of 500 °C is also consistent with the observations of Nord (1976) that the anti-phase domains formed in anorthite in sample 76535 during the $I\bar{1} \rightarrow P\bar{1}$ transition are comparable in size (~100 nm) to those observed in basalts.

It appears likely that, subsequent to a period of slow cooling in a plutonic environment, 76535 underwent a period of more rapid cooling leading to closure temperatures for cation ordering of ~500 °C. Troctolite 76535 was a loose soil sample collected as part of the station 6 rake sample but the timing and mechanism of its transportation to the surface from deep in the Moon are poorly constrained. The most plausible explanation of the thermobarometric and cooling rate data on 76535 is the sample was excavated from an intrusion deep within the lunar crust by a basin-forming impact *before* it cooled below the closure temperature (~500 °C) indicated by the Fe–Mg ordering in orthopyroxene. Subsequent cooling took place in the ejecta blanket close to the lunar surface.

Ages determined for 76535 have a bearing on the problem because, unlike 76255, they preserve a pre-Serenitatis age. Sm–Nd (4260 ± 60 Ma, Lugmair et al., 1976), U–Pb (4236 ± 15 Ma, Premo and Tatsumoto, 1992), Pb–Pb (4226 ± 35 Ma, Premo and Tatsumoto, 1992) and Ar–Ar

(4230 Ma, Huneke and Wasserburg, 1975) ages form a tight cluster representing the time of closure of these systems. If the radiometric clocks started at the time of excavation this implies that the system was isotopically open prior to excavation. Given that the closure temperature of the Sm–Nd isotopic system for plagioclase is ~600 °C (Ganguly and Tirone, 2001), 76535 must have been at a temperature $\geqslant$600 °C at the time of excavation. The Rb–Sr age of 4510 ± 70 Ma (Papanastassiou and Wasserburg, 1976), which is based largely on inclusions in olivine, appears problematic unless it represents the original crystallization age. Papanastassiou and Wasserburg (1976) proposed that olivine crystals acted as inert containers preventing isotopic exchange between inclusions with high Rb–Sr values and the matrix during cooling. This model is supported by evidence of in situ decay of ^{244}Pu leading to Xe retention ages of 4.50 Ga for olivine separates and 4.25 Ga for plagioclase separates from 76535 (Caffee et al., 1981). The possibility remains, however, that the Rb–Sr "age" may be an artifact of recent Rb loss from olivines in proportions that resulted in a 4510 Ma pseudo-isochron (Premo and Tatsumoto, 1992).

If the Rb–Sr age is the original crystallization age, ~250 million years elapsed before the other isotope systems closed. This is not inconsistent with a lunar crust kept hot by heat diffusing from the KREEP-rich zones at the base of the crust. The KREEP-rich zones have elevated U, Th and K contents and thermal calculations indicate that these KREEPy zones would remain at solidus or near-solidus temperatures for hundreds of millions of years after primary lunar differentiation. It is worth recalling that, although 76535 formed initially as an igneous cumulate, it has been thoroughly metamorphosed as indicated by the texture of the rock and its equilibration temperature of 800 °C. Stewart (1975) originally suggested that 76535 was the type example of "Apollonian metamorphism", an event that lasted for at least $>10^8$ years after lunar differentiation was complete. Most plausibly, the Sm–Nd, Pb–Pb and Ar–Ar ages represent the time of excavation of this sample from the deep crust while the sample was at a temperature above 500 °C and the cooling rate of 0.04 °C/year obtained from the orthopyroxene chronometer represents cooling at a depth of around 200 m in the ejecta blanket produced during the impact event that brought 76535 to the surface.

6. Conclusions

Cation ordering states of pyroxenes have the potential to reveal the duration and nature of processes that take place at relatively low temperatures and thus they provide a useful tool in deciphering the latest stages of the complex thermal histories of planetary samples. Diffusion-controlled processes of inter-crystalline cation exchange, intra-crystalline exsolution, and intra-crystalline Fe–Mg ordering occur on different spatial and temporal scales and they record different events in the evolution of rocks with complex thermal histories. In intra-crystalline cation ordering, the diffusion path length is short and the corresponding closure temperature is low. Plutonic rocks that have been cooled extremely slowly or that have been subjected to low temperature metamorphism will tend to anneal and equilibrate during the cooling process and give low closure temperatures for the cation ordering process, as shown by the data on the orthopyroxene from the Stillwater Complex. Lunar Mg-suite plutonic samples 76255 and 76535 give relatively high closure temperatures for cation ordering, indicating an interruption of the slow plutonic cooling process. The most effective mechanism to cause this interruption is by "quenching" due to a large impact. Pre-excavation thermal history is more difficult to determine. However, samples 76255 and 76535 appear to have had different thermal histories. 76255 crystallized initially in a high level intrusion within a few kilometers of the lunar surface and had cooled well below the closure temperature for isotopic systems at the time of its excavation. On the other hand, thermobarometric and geochronologic data indicate that 76535 formed deep within the Moon and remained above the closure temperature for isotopic systems until it was excavated at 4.25 Ga, at which point the isotopic clocks started. Considered in conjunction with geochronologic data from different isotopic systems, mineralogically based thermal histories provide useful constraints on models of planetary thermal and magmatic evolution.

Acknowledgments

This paper is dedicated to the memory of Larry Haskin. Larry contributed greatly to lunar science from the earliest pre-Apollo days and his creative and thoughtful approach to important lunar and terrestrial problems was an inspiration to all of us. This work has been supported by NASA Grants NAG5-11587 and NNG05GH36G and by the Italian project Cofin 2001 "Structural evolution and phase transitions in minerals as a function of temperature, pressure and composition". We thank M. Mellini for providing access to the TEM facilities at Siena University. The manuscript benefited from reviews by Brad Jolliff, John Longhi, Clive Neal and an anonymous reviewer.

Associate editor: Clive R. Neal

Appendix A. Supplementary data

Supplementary data associated with this article can be found, in the online version, at doi:10.1016/j.gca.2006.08.009.

References

Cadogan, P.H., Turner, G., 1976. The chronology of the Apollo 17 station 6 boulder. In: Proc. Lunar Sci. Conf. 7th, pp. 2267–2285.

Caffee, M., Hohenberg, C.M., Hudson, B., 1981. Troctolite 76535: a study in the preservation of early isotopic records. In: Proc. Lunar Planet. Sci. Conf. 12th, pp. 99–115.

Cámara, F., Doukhan, J.C., Domeneghetti, M.C., Zema, M., 2000. A TEM study of Ca-rich orthopyroxenes with exsolution products: implications for Mg–Fe ordering process. *Eur. J. Mineral.* **10**, 735–748.

Champness, P.E., Lorimer, G.W., 1973. Precipitation (exsolution) in an orthopyroxene. *J. Mater. Sci.* **8**, 467–474.

DePaolo, D.J., Wasserburg, G.J., 1979. Sm–Nd age of the Stillwater Complex and the mantle evolution curve for neodymium. *Geochim. Cosmochim. Acta* **43**, 999–1008.

Dollase, W.A., Newman, W.I., 1984. Statistically most probable stoichiometric formulae. *Am. Mineral.* **69**, 553–556.

Domeneghetti, M.C., Molin, G.M., Tazzoli, V., 1995. A crystal-chemical model for Pbca orthopyroxene. *Am. Mineral.* **80**, 253–267.

Domeneghetti, M.C., Tazzoli, V., Boffa Ballaran, T., Molin, G.M., 1996. Orthopyroxene from the Serra De Magé meteorite: a structure refinement procedure for a Pbca phase coexisting with a C2/c exsolved phase. *Am. Mineral.* **81**, 842–846.

Dymek, R.F., Albee, A.L., Chodos, A.A., 1975. Comparative petrology of lunar cumulate rocks of possible primary origin: dunite 72415, troctolite 76535, norite 78235, and anorthosite 62237. In: Proc. Lunar Sci. Conf. 6th, pp. 301–341.

Ganguly, J., 1982. Mg–Fe order-disorder in ferromagnesian silicates: II. Thermodynamics, kinetics and geological applications. In: Saxena, S.K. (Ed.), *Advances in Physical Geochemistry*. Springer, New York, pp. 88–99.

Ganguly, J., Domeneghetti, M.C., 1996. Cation ordering of orthopyroxenes from the Skaergaard Intrusion: implications for the subsolidus cooling rates and permeabilities. *Contrib. Mineral. Petrol.* **122**, 359–367.

Ganguly, J., Tazzoli, V., 1994. Fe^{2+}–Mg interdiffusion in orthopyroxene: retrieval from the data on intracrystalline exchange reaction. *Am. Mineral.* **79**, 930–937.

Ganguly, J., Tirone, M., 2001. Relationship between cooling rate and cooling age of a mineral: theory and application to meteorites. *Meteorit. Planet. Sci.* **36**, 167–175.

Ganguly, J., Bhattacharya, R.N., Chakraborty, S., 1988. Convolution effect in the determination of compositional profiles and diffusion coefficients by microprobe step scans. *Am. Mineral.* **73**, 901–909.

Huneke, J.C., Wasserburg, G.J., 1975. Trapped ^{40}Ar in troctolite 76535 and evidence for enhanced ^{40}Ar–^{39}Ar plateaus. *Lunar Sci. VI*, 417–419.

Ibers, J.A., Hamilton, W.C. (Eds.), 1974. International Tables for X-ray Crystallography, vol. 4. Kynoch Press, Birmingham, UK, pp. 99–101.

Irvine, T.N., 1970. Heat transfer during solidification of layered intrusions. I. Sheets and sills. *Can. J. Earth Sci.* **7**, 1031–1061.

Jolliff, B.L., Floss, C., McCallum, I.S., Schwartz, J.M., 1999. Geochemistry, petrology, and cooling history of 14161,7373: a plutonic lunar sample with textural evidence of granitic-fraction separation by liquid immiscibility. *Am. Mineral.* **84**, 821–837.

Lehmann, M.S., Larsen, F.K., 1974. A method for location of the peaks in step-scan measured Bragg reflections. *Acta Crystallographica* **A30**, 580–584.

Lugmair, G.W., Marti, K., Kurtz, J.P., Scheinin, N.B., 1976. History and genesis of lunar troctolite 76535 or: How old is old? In: Proc. Lunar Planet. Sci. Conf. 7th, pp. 2009–2033.

McCallum, I.S., O'Brien, H.E., 1996. Stratigraphy of the lunar highland crust: depth of burial of lunar samples from cooling rate studies. *Am. Mineral.* **81**, 1166–1175.

McCallum, I.S., Schwartz, J.M., 2001. Lunar Mg suite: thermobarometry and petrogenesis of parental magmas. *J. Geophys. Res.* **106**, 27969–27983.

McCallum, I.S., Thurber, M.W., Nelson, B.K., O'Brien, H.E., 1999. Lead isotopes in sulfides from the Stillwater Complex, Montana: evidence for subsolidus remobilization. *Contrib. Mineral. Petrol.* **137**, 206–219.

Mueller, R.F., 1967. Model for order-disorder kinetics in certain quasibinary crystals of continuously variable composition. *J. Phys. Chem. Solids* **28**, 2239–2243.

Nord Jr., G.L., 1976. 76535: Thermal history deduced from pyroxene precipitation in anorthite. In: Proc. Lunar Planet. Sci. Conf. 7th, pp. 1875–1888.

Nord Jr., G.L., 1980. The composition, structure, and stability of Guinier-Preston Zones in lunar and terrestrial orthopyroxene. *Phys. Chem. Minerals* **6**, 109–128.

North, A.C.T., Phillips, D.C., Mathews, F.S., 1968. A semi-empirical method of absorption correction. *Acta Crystallographica* **A24**, 351–359.

Papanastassiou, D.A., Wasserburg, G.J., 1976. Rb–Sr age of troctolite 76535. In: Proc. Lunar Planet. Sci. Conf. 7th, pp. 2035–2054.

Premo, W.R., Tatsumoto, M., 1992. U–Th–Pb, Rb–Sr, and Sm–Nd isotopic systematics of lunar troctolitic cumulate 76535: implications on the age and origin of this early, deep-seated cumulate. In: Proc. Lunar Planet. Sci. Conf. 22nd, pp. 381–397.

Sack, R.O., Ghiorso, M.S., 1994. Thermodynamics of multicomponent pyroxenes II. Applications to phase relations in the quadrilateral. *Contrib. Mineral. Petrol.* **116**, 287–300.

Sheldrick, G.M., 1998. *Programs for Crystal Structure Analysis (Release 97-2)*. Institüt für Anorganische Chemie der Universität, Göttingen, Germany.

Simonds, C.H., Phinney, W.C., Warner, J.L., 1974. Petrography and classification of Apollo 17 non-mare rocks with emphasis on samples from the station 6 boulder. In: Proc. Lunar Science Conf. 5th, pp. 337–353.

Smyth, J.R., 1974. Low orthopyroxene from a lunar deep crustal rock: a new pyroxene polymorph of space group $P2_1ca$. *Geophys. Res. Lett.* **1**, 27–29.

Smyth J.R., 1975. Intracrystalline cation order in a lunar crustal troctolite. In: Proc. Lunar Planet. Sci. Conf. 6th, pp. 821–832.

Steele, I.M., 1975. Mineralogy of lunar norite 78235: second lunar occurrence of $P2_1$ ca pyroxene from Apollo 17 soils. *Am. Mineral.* **60**, 1086–1091.

Stewart, D.B., 1975. Apollonian metamorphic rocks: the products of prolonged subsolidus equilibration. *Lunar Sci. VI*, 774–776.

Stimpfl, M., 2005. The Mn, Mg-intracrystalline exchange reaction in donpeacorite ($Mn_{0.54}Ca_{0.03}Mg_{1.43}Si_2O_6$) and its relation to the fractionation behaviour of Mn in Fe, Mg-orthopyroxene. *Am. Mineral.* **90**, 155–161.

Stimpfl, M., Ganguly, J., Molin, G., 1999. Fe–Mg order-disorder in orthopyroxene: equilibrium fractionation between the octahedral sites and thermodynamic analysis. *Contrib. Mineral. Petrol.* **136**, 297–309.

Stimpfl, M., Ganguly, J., Hervig, R. (2003). Ca and Mg tracer diffusion in diopside: experimental determination and applications to cooling history of planetary samples. Lunar Planet. Sci. vol. XXXIV. Lunar Planet. Inst., Houston, #1497 (abstract).

Stimpfl, M., Ganguly, J., Molin, G., 2005. Kinetics of Fe^{2+}-Mg order-disorder in orthopyroxene: experimental studies and applications to cooling rates of rocks. *Contrib. Mineral. Petrol.* **150**, 319–334.

Warner, J.L., Simonds, C.H., Phinney, W.C., 1976. Apollo 17, Station 6 boulder sample 76255: absolute petrology of breccia matrix and igneous clasts. In: Proc. Lunar Sci. Conf. 7th, pp. 2233–2250.

Warren, P.H., Haack, H., Rasmussen, K.L., 1991. Megaregolith insulation and the duration of cooling to isotopic closure within differentiated asteroids and the Moon. *J. Geophys. Res.* **96**, 5909–5923.